Construction and Building Materials 512 (2026) 145154

Contents lists available at ScienceDirect

Construction and Building Materials

journal homepage: www.elsevier.com/locate/conbuildmat

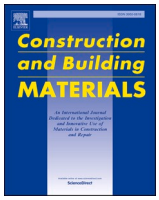

# Lithium silicate as a healing agent in vascular networks for natural hydraulic lime mortars: a step towards cyclic self-healing systems for heritage materials

C. De Nardi *, D. Gardner

*Resilient Structures and Construction Materials (RESCOM) Research Group, School of Engineering, Cardiff University, Queen's Buildings, The Parade, Cardiff, Wales CF243AA, United Kingdom*

ARTICLE INFO

*Keywords:*
Built heritage
Self-healing
Lime-based mortars
Cyclic healing
Lithium silicates
Vascular networks

ABSTRACT

Built heritage is increasingly exposed to diverse and intense environmental stressors as a consequence of climate change. Consequently, historic masonry repair strategies must evolve to support a more resilient and long-lasting preservation approach. Drawing on biomimetic principles, recent innovations have introduced vascularisation techniques to enable autonomous crack repair in lime-based mortars, including targeted patching applications where localized material loss needs to be effectively restored. However, the effectiveness of these self-healing systems depends largely on the performance of the healing agents, particularly their long-term reactivity and compatibility with traditional materials. This study evaluated lithium silicate solutions, LS15 and LS20 (15 % and 20 % lithium wt. respectively) as healing agents in natural hydraulic lime mortars using simplified vascular networks. Samples were pre-cracked to a crack width of 0.1 mm and were allowed to heal over 14 days. Three-point bending tests were conducted to assess mechanical recovery at 14, 28, and 365 days, including up to three damage–healing cycles for long-term evaluation. No significant autogenous healing was observed in the control specimens. LS20 achieved maximum single-cycle strength and stiffness recovery of 187 % and 124 %, respectively, at early age. Over multiple cycles, in samples aged 1 year, LS15 showed greater consistency, reaching up to 68 % strength and 51 % stiffness recovery by the third cycle. These results demonstrate lithium silicate's potential for repeatable, cyclic self-healing in heritage-compatible mortars.

## 1. Introduction

As climate change accelerates, its effect on the built environment—particularly on historic structures—is becoming increasingly pronounced. Historic structures constructed with traditional materials such as masonry, clay, natural stone, and lime-based mortars are particularly susceptible to environmental deterioration due to their high porosity, vapor permeability, and relatively low mechanical strength [1–3]. Mortars, being the most vulnerable component in masonry, typically deteriorates faster than the units it binds. Lime-based mortars, common in historic buildings, are especially susceptible to erosion, salt crystallization, freeze–thaw cycles, biological colonisation and mechanical stresses [4,5]. These deterioration mechanisms have been increasingly exacerbated by the effects of climate change, including more frequent extreme weather events, increased rainfall intensity, temperature fluctuations, and rising humidity levels [6,7]. The degradation of mortar joints leads to loss of cohesion between masonry units, reduced structural integrity, and increased permeability of the wall system. Over time, this can cause disaggregation of the masonry, uneven load distribution, and acceleration of decay in adjacent materials [8,9].

Among traditional binders, natural hydraulic lime (NHL) mortars are widely preferred in restoration contexts due to their chemical and physical compatibility with historic materials [10], [11]. NHL's mineral composition creates a strong bond with historic masonry, reducing the risk of damaging interactions like cracking or salt accumulation [12]. Furthermore, Natural Hydraulic Lime (NHL) mortars, such as NHL 3.5, are classified as moderately hydraulic, meaning they develop strength through both hydration and carbonation mechanisms at a balanced rate, resulting in a progressive increase in mechanical strength over time. Despite this gradual hardening, NHL mortars retain lower stiffness and compressive strength compared to most historic masonry units, enabling

* Corresponding author.
*E-mail address:* denardic@cardiff.ac.uk (C. De Nardi).

https://doi.org/10.1016/j.conbuildmat.2026.145154
Received 14 August 2025; Received in revised form 30 November 2025; Accepted 5 January 2026
Available online 23 January 2026

them to act as sacrificial materials [12,13]. Recent experiments also confirm that NHL mortars possess a more porous microstructure characterised by larger pore sizes and higher overall porosity, which contributes to their higher ductility and lower strength relative to Portland Cement mortars [14]. This mechanical and microstructural compatibility reduces stress concentrations and mitigates damage to the original masonry elements, thereby supporting the long-term preservation of historic structures under environmental and structural loads [15,16].

Recent research highlights the urgent need for adaptive measures to protect built heritage from the escalating impacts of climate change. A combination of traditional solutions, adaptive technologies borrowed from modern construction, and novel emerging methods can be employed to preserve and reinforce heritage structures [17]. Among these, biodesign innovations—such as microbial-enhanced, carbon--fixing limewash—show promise in enhancing the resilience of traditional materials without altering their historic character [18]. Digital prototyping and regenerative design approaches are being increasingly integrated with climate data and predictive modelling to strengthen the adaptive capacity of both cultural and natural heritage sites [19].

To support this shift, comprehensive frameworks for climate-resilient materials are emerging, including self-healing technologies [20]. Self-healing materials are engineered systems that can autonomously detect and repair damage, such as microcracks, to restore their structural or functional integrity [21]. Inspired by biological systems—known for their innate ability to repair themselves after damage—self-healing materials are designed to enhance durability, extend service life, and reduce maintenance requirements [22,23]. In the context of heritage conservation, a range of self-healing strategies is currently being explored. These include autogenous self-healing, which relies on the intrinsic ability of binder materials to close cracks through continued hydration and carbonation [24–26]; bio-based healing agents [27], miniaturised vascular networks embedded in mortars [28,29], and autonomous crack repair mechanisms [24,30] to enhance the performance of repair materials while preserving the authenticity and integrity of historic structures. Biological self-healing methods, such as microbial-induced calcium carbonate precipitation (MICP), have demonstrated effective crack repair through biomineralisation processes and are increasingly gaining attention as a promising solution. However, recent studies have highlighted challenges—including high costs, scalability issues regulatory gaps, and inconsistent performance across environments—that limit MICP's widespread adoption [31–33]. Among construction materials, cementitious composites have been widely studied for their self-healing potential [34–37], with one advanced approach focusing on the integration of vascular networks—extrinsic self-healing systems inspired by biological circulatory systems [38–40]. These networks consist of interconnected hollow channels or tubes embedded within the concrete matrix, acting as artificial "veins" that transport healing agents—such as mineral solutions [41,42], or adhesives [43,44]—directly to sites of damage. Since Dry's pioneering work with embedded glass tubes, the concept has evolved significantly through various fabrication strategies [22,23]. Hollow tubes (glass, plastic, or metal) offer simplicity but can be prone to clogging and may compromise structural strength [45–48]. Sacrificial materials, including dissolvable polymers or wax-based elements, provide better integration into the matrix but require removal processes [49–51]. 3D printing technologies enable the creation of precise, interconnected channels although their implementation can present challenges in terms of cost and technical complexity [38,52]. Notably, researchers at Cardiff University [43,53] have developed a practical method for generating 2D vascular systems by embedding and later removing polyurethane tubes, forming interconnected channels within cementitious materials—an approach that has been successfully validated through full-scale site trials [54]. When microcracks form and intersect the network, the rupture of the channels releases the healing agent, which then fills the crack and solidifies, restoring the material's integrity. Importantly, these systems can be designed for repeated healing cycles, either through passive capillary flow or active pumping of the healing agent from external reservoirs [44].

Selecting an appropriate healing agent is crucial to optimising the vascular system's performance. It needs to provide long-term stability while facilitating the mortar matrix's natural self-repair mechanisms. Key properties include low viscosity and compatibility with historic materials—this ensures the agent can efficiently navigate the vascular network and thoroughly penetrate cracks. Moreover, the agent must be non-toxic to guarantee environmental safety and suitability for construction applications.

In this context, inorganic consolidants—particularly silicate-based systems—have shown promise for stabilising and strengthening porous, binder materials [55,56]. Sodium silicate is well-known for its self-healing ability in concrete structures [56–61]. When utilised within vascular networks, sodium silicate serves as an effective healing agent, facilitating the restoration of structural integrity in damaged concrete [41,48]. The healing efficiency of sodium silicate depends on several factors, including its concentration, viscosity, and the environmental conditions of the concrete system [57]. The $SiO_2$ in the healing agent reacts with calcium hydroxide from the hydrated cement paste to produce C–S–H (tobermorite) gel, which is the primary binding phase in hydrated cement [62,63]. Studies have shown that sodium silicate-based systems can achieve up to 80–90 % recovery in mechanical strength and permeability reduction after cracking, demonstrating its potential for structural applications [64,65].

Compared to calcium silicate, sodium silicate, and potassium silicate, lithium silicate (LS) has the lowest formula unit weight [66–68]. Unlike other silicate treatments such as ethyl silicate, which form silica gels through polymerisation, lithium silicate reacts directly with calcium ions to form calcium-silicate-hydrate (C-S-H) phases [69,70]. These phases densify the pore structure and enhance mechanical properties [71,72]. Lithium silicates are also found in water glass, which is widely used for the surface treatment of cement-based materials and as an inorganic coating for concrete pavements. Moreover, when applied to concrete surfaces, LS has been found to improve wear and frost resistance, ultimately extending the service life of concrete pavements [71]. Furthermore, incorporating 2–10 % LS into Portland cement significantly increases C-S-H formation and accelerates setting time, while even a 1.0 % addition slightly enhances setting and early-stage flexural and compressive strengths [73].

Such characteristics make lithium silicate a compelling option not only for consolidation purposes but also as a functional healing agent in vascular technology within lime-based mortar matrices.

Wettability (contact angle / spreading behaviour) is closely linked to the transport of healing agents into cracks, which is a key determinant of extrinsic self-healing efficiency. In systems where healing agents are released via capsules or vascular networks, good wettability ensures that, once released, the liquid can spread along and adhere to crack surfaces, infiltrate narrow fissures through capillary forces, and react with the surrounding matrix to form solid healing products that fill and seal the crack [39,74]. Poor wettability may inhibit this process, limiting the penetration of the healing agent into the crack and reducing the formation or deposition of healing products along the crack surfaces. Moreover, literature shows that healing is most effective for narrower cracks (microcracks) where capillary transport, aided by wettability, can realistically deliver reactants to all surfaces [75]. Hydration, continued chemical reaction with unreacted silicates or lime, and formation of calcium carbonate or calcium silicate hydrate phases are mechanisms that depend on sufficient contact and transport of liquid-phase reactants. Thus, measuring the contact angle of healing agents provides useful predictive information on their ability to be delivered into cracks and contribute to healing or sealing under realistic environmental conditions [76,77].

A recent comparative study by Song et al. [78] directly evaluated the effects of lithium silicate on NHL mortars, applying the treatment via impregnation and surface spraying (0.2 $kg/m^2$). The results

demonstrated remarkable improvements in mechanical and durability performance: compressive strength increased by 32.7–52.0 %, surface hardness improved by 10 grading units, and weight loss under freeze–thaw cycling decreased by 31.6–43.8 %. Microstructural analyses revealed a reduction in macroporosity and a corresponding increase in meso- and nanopores, suggesting that lithium silicate not only fills but also refines the pore network, potentially enhancing capillary resistance and reducing ingress of harmful salts. In addition to their densifying capabilities, lithium silicate solutions have been explored for their potential in self-healing applications within cementitious materials. Research indicates that encapsulating lithium silicate in microcapsules promotes C-S-H formation, seals microcracks, and improves concrete durability [79], a process further supported by Stępień et al. [80] who demonstrated the participation of Lithium Silicate in the transformation of calcium hydroxide (CH) into new calcium silicate hydrate (C-S-H) gel, as shown in Eq. (1).

$$Li_2O{\cdot}nSiO_2 + mH_2O + nCa(OH)_2 \rightarrow nCaO{\cdot}SiO_2{\cdot}(m + n - 1)H_2O + 2LiOH \quad (1)$$

As highlighted by Song et al. [78] in this reaction, lithium silicate reacts with calcium hydroxide and water to form additional calcium silicate hydrate gel, with lithium hydroxide (LiOH) formed as a byproduct. The newly formed C-S-H contributes to the densification of the microstructure by filling capillary pores and reducing porosity, which in turn enhances the mechanical performance of the silicate-based material [81]. The consumption of calcium hydroxide also decreases the CH content in the hardened matrix, which is typically associated with improved durability and mechanical stability. This pozzolanic-like reaction underpins the healing mechanism of lithium silicate: upon infiltration into cracks, the solution interacts with $Ca(OH)_2$ present in the hydrated lime matrix to form C–S–H phases that progressively fill and bridge microcracks, restoring mechanical continuity. This mineral-based healing process is analogous to secondary hydration, where the newly formed products effectively seal cracks and contribute to stiffness recovery [82]. Studies have highlighted that, compared to other silicates such as sodium or potassium silicates, the smaller size and higher mobility of $Li^+$ ions [73,82] enable deeper penetration into the fine pore structure of natural hydraulic lime mortars and promote a faster, more homogeneous formation of calcium–silicate–hydrate (C-S-H) phases [69,78,83]. Moreover, sodium and potassium silicates may leave residual alkalis that contribute to efflorescence on porous lime substrates [66], while $Li^+$ ions' limited mobility favours stronger interactions with hydration products, improving absorption [84]. Interestingly, Song et al. [78] reported that lithium silicate pretreatment of NHL-based mortars significantly enhanced durability, with treated samples exhibiting a 31.6–43.8 % reduction in weight loss during freeze-thaw cycles compared to controls. The treatment reduced macropore content (50–10,000 nm), increased mesopores and nanopores, and formed a protective silicate coating on the surfaces through rehydration processes that generated C-S-H gel [78].

These attributes make lithium silicate solutions suitable for integration into self-healing vascular networks, thereby contributing to both the durability and sustainability of structures. In this context, ongoing research by the authors [28] focuses on designing vascular networks that can be fully embedded within mortar joints while ensuring chemo-physical and mechanical compatibility.

Vascular networks can be integrated into traditional masonry repair techniques such as patching. When extensive portions of masonry have deteriorated to the extent that the mortar joints can no longer perform their structural role, the scuci-cuci (patching) technique can be employed. This method restores structural continuity while preserving the original masonry fabric. In this approach, renewed hydraulic lime-based mortar joints are embedded with vascular networks filled with healing agents. In this context, the careful selection of appropriate healing agents is crucial. The choice directly influences not only the compatibility and effectiveness of the self-healing process but also the potential to enhance the system's functionality, for instance, network refilling mechanisms that allow for repeated healing cycles, or self-sensing activation that triggers repair automatically upon detecting damage.

The objective of this paper is to assess the self-healing performance of lithium silicate solutions by evaluating two concentrations (15 % and 20 % by weight in water), with the aim of determining their efficacy and reliability in promoting effective and repeatable crack healing in natural hydraulic lime mortars. To enable meaningful comparison, a well-established approach was used for vascular network formation (as summarised in Section 2.1) [43,44]. The healing efficacy was analysed with respect to a controlled crack width of 0.1 mm and a fixed healing period of 14 days. Prismatic samples were tested at different curing ages: 14 and 28 days, representing early-age cracking, and after 1 year, representing medium- to long-term behaviour. Both single and multiple (up to three) damage–healing cycles were considered for selected specimens to evaluate the repeatability of the self-healing performance and its durability over time. Initially, the wetting characteristics of the healing agents were evaluated through contact angle measurements. Subsequently, the healing performance was assessed in terms of flexural strength and stiffness recovery using three-point bending tests.

## 2. Materials and methods

### 2.1. Essential background – specimen manufacturing and testing

A well-established method originally developed by Davies et al. [43,44,85] for concrete was adapted in this study to create vascular networks in natural hydraulic lime (NHL) mortars. Polyethylene terephthalate (PET) tubes (4 mm diameter) were embedded into prismatic NHL samples and removed after 7 days to form internal channels (Fig. 1). This process enables the formation of hollow channels that allow direct contact between the healing agents and the mortar matrix, thereby isolating the healing performance from any external influences and ensuring that observed effects can be attributed solely to the agents themselves. Mortar samples were prepared using NHL 3.5 (supplied by Tarmac) and 0–2 mm sand at a 1:3 binder-to-sand and 1:0.7 water-to-lime ratio, as commonly used for historical mortars [86–88]. A series of 75 × 75 × 255 mm prisms, as represented in Fig. 1(a)) were cast in three layers, with PET tubes placed in the bottom layer (Fig. 1(b)). After casting, samples were kept in the moulds covered with a damp Hessian sheet for seven days and subsequently demoulded and stored in laboratory environmental conditions (20° ± 5, RH ~ 45 %) up to the first test. Before the test, a central notch was created to guide crack formation during three-point bending tests. To monitor crack development, CMOD clip gauges were installed, with a loading rate of 0.0001 mm/s applied consistently during the test. Further details on raw materials, casting, mixing, and testing procedures can be found in [28,43,44].

### 2.2. Healing agents

The healing agents were injected into the pre-formed vascular channels immediately after crack formation (as detailed in Section 2.4, Stage 2). Each channel received 4 mL of the lithium silicate solution (LS15 or LS20) using a syringe. Once the cracks intersected the channels, the solutions were drawn into the damaged zones by capillary action, enabling targeted delivery and minimizing external influences.

Two aqueous lithium silicate (LS) solutions were prepared by dilution of a commercial concentrate (28 wt% active ingredient), supplied by Chimica Restauri. The solutions were formulated to obtain final concentrations of 15 wt% and 20 wt% active lithium silicate, hereafter referred to as LS15 and LS20, respectively. These concentrations were selected based on preliminary experiments indicating that they offered better healing efficiency in NHL mortars than higher-concentration

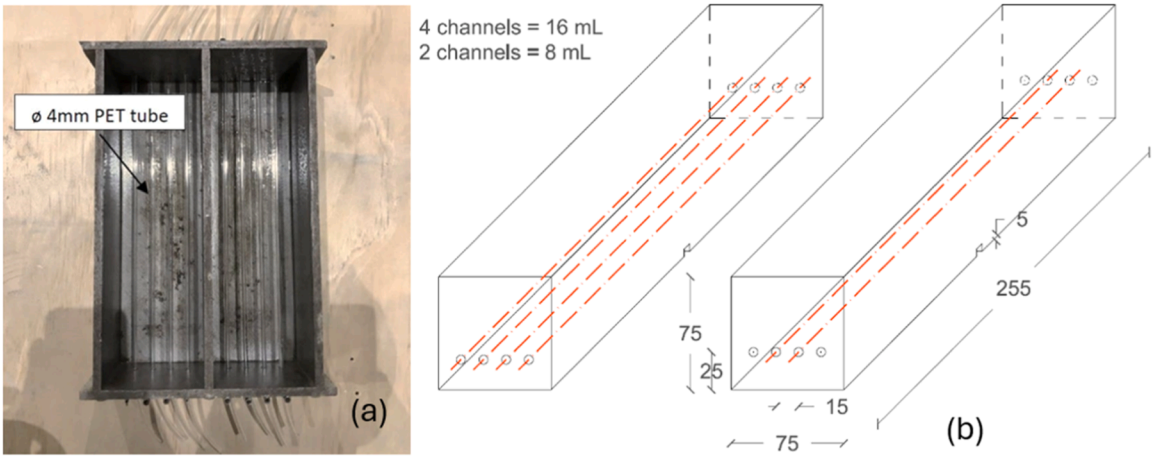


**Fig. 1.** Specimen preparation with twin moulds before casting (a) samples dimensions (b).

formulations of the same product, i.e. 24 % and 28 %, which tended to increase viscosity and reduce penetration, making them less suitable for vascular delivery. Assuming that the density of the 28 wt% stock solution is approximately equal to that of water (1 g/mL), the following dilutions were carried out based on volume ratios. LS15: Approximately 540 mL of the 28 wt% stock solution was diluted with 460 mL of deionized water, yielding a total volume of ~1000 mL and a final concentration of approximately 15 wt%. LS20: for the preparation of LS20, approximately 700 mL of the 28 wt% concentrate was diluted with 300 mL of deionized water, resulting in a total volume of ~1000 mL and a final concentration of approximately 20 wt%. Dilution ratios were based on volume measurements, while concentrations refer to weight percent of active lithium silicate.

### 2.3. Analysis of wettability

Dynamic contact angle (SCA) measurements were carried out over a 10-second period using a contact angle goniometer (DataPhysics OCA100, Germany) equipped with a camera-based optical measurement system. All measurements were performed at room temperature (20 ± 5 °C) and approximately 50 % relative humidity. Glass microscope slides (22 × 50 × 0.15 $mm^3$; Deckgläser, Menzel-Gläser, Germany) were used as substrates, offering a smooth, inert, and reproducible surface for assessing the intrinsic wettability of the healing agents. This setup was preferred because porous substrates, such as natural hydraulic lime mortar, could lead to rapid liquid absorption, compromising accurate and comparable measurement of the initial wetting behaviour. A 0.5 µL droplet of test liquid was placed on the surface, and once equilibrium was reached, its shape was captured by the camera. The contact angle was then calculated using the SCA20 software (DataPhysics), based on the captured image. The reported SCA represents the average of the left and right contact angles.

### 2.4. Experimental arrangement and programme

Three curing durations were considered: 14 and 28 days to represent the short term, and 1 year to represent the medium-to-long term. Following curing, the prisms were either loaded to failure (control series) or subjected to a three-point bending test, in accordance with BS EN 12390–5 [89], until a specified crack mouth opening displacement (CMOD) of 0.1 mm was reached, after which they were unloaded. The CMOD threshold of 0.1 mm was chosen as it represents the maximum permissible damage level, beyond which larger cracks would lead to specimen failure. Fig. 2 illustrates the vascular network system and the flexural test setup.

All three-point bending tests were performed using an Instron 8871 universal testing machine (Instron, England, UK), equipped with a 100 kN load cell and CMOD clip gauge.

The flexural test configuration is illustrated in Fig. 3(b) and a cyclic loading and healing protocol was designed to evaluate the self-healing capacity of the material. The procedure included five stages:

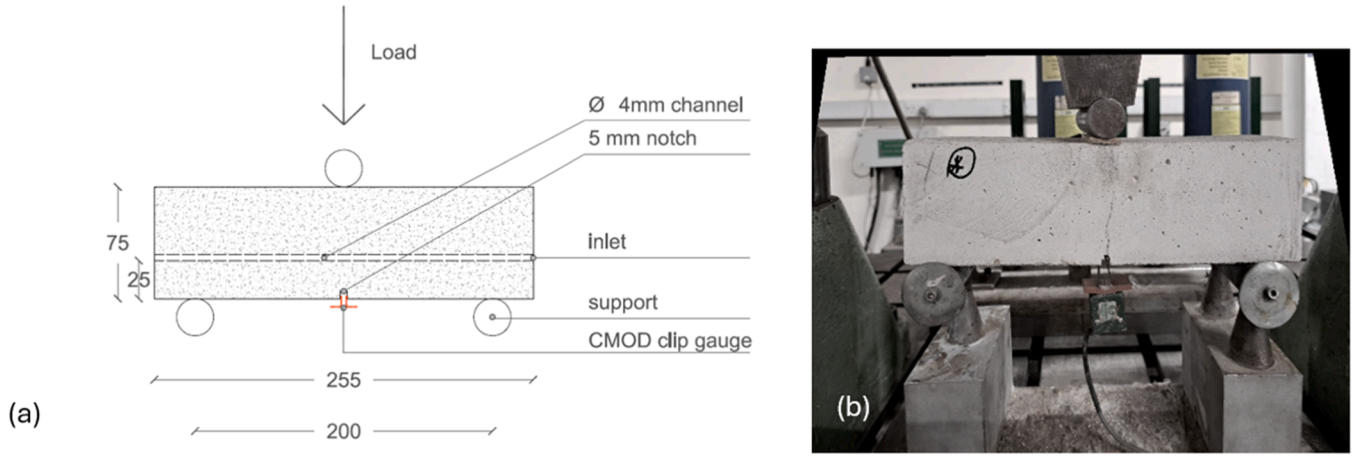


**Fig. 2.** Schematic representation of the three-point bending test setup on notched beam specimens (a), Experimental setup showing the test in progress with the loading applied at midspan and CMOD gauge installed at the notch (b).

- Stage 1: specimens were subjected to a three-point bending test until a CMOD of 0.10 mm was reached. This induced microcracking and mechanical degradation, as shown by the solid red curve in Fig. 3 (first test).
- Stage 2: following the initial damage, specimens were injected with the selected healing agent and placed under laboratory environmental conditions (20 ± 5 °C, RH ~45 %) for a 14-day healing period. The healing agents were injected at this stage to simulate their release upon damage, thereby avoiding premature absorption by the matrix prior to crack formation, similar to the mechanism observed in comparable self-healing systems where the healing agent is released from its point of encapsulation once a threshold damage is exceeded.
- Stage 3: specimens were reloaded under a three-point bending test to a CMOD value of 0.10 mm. They were then re-filled with the same volume of healing agent used in Stage 2, or less if any channels were blocked, noting the volume injected, and returned to the same environmental conditions (20 ± 5 °C, RH ~45 %) for an additional 14-day healing period.
- Stage 4: a third loading cycle was carried out following the same procedure and the specimens re-filled using the same method described in Stage 3. The material response after this second healing cycle is represented by the dash-dot and dotted red lines in Fig. 3.
- Stage 5: after the last 14-day healing period, specimens underwent a final flexural test in which they were loaded to failure.

The experimental programme, as presented in Table 1 can be divided into three main groups. The aim of Group 1 was twofold: first, to assess whether the pure natural hydraulic lime mortar (control) exhibits any autogenous healing properties at an early age (i.e., after 14 days of curing); and second, to evaluate the healing performance achieved when lithium silicate solutions LS15 and LS20 were used to fill either two or four channels. Similarly, in Group 2, the curing time was extended to 28 days, a single healing cycle was considered, and the same CMOD value of 0.10 mm was applied. The aim of Group 3 was to analyse the healing behaviour over the medium to long term, specifically to determine whether natural autogenous healing remained appreciable after one year of curing and whether the lithium silicate solutions could still react with the matrix at that stage. In this group, samples were filled with the maximum volume (i.e., four channels) using both silicate solutions (LS15 and LS20), and multiple damage–healing cycles were applied. The CMOD was consistently maintained at 0.10 mm, with a healing period of 14 days for each cycle.

Fragments from the crack surfaces of Group 3 samples were examined using scanning electron microscopy (SEM) at Cardiff University, employing a Zeiss Sigma HD Field Emission Gun Analytical SEM (ASEM) fitted with an in-lens and Everhart–Thornley secondary electron detector, as well as a backscatter electron detector.

Three prisms were cast for each sample designation. The sample designation is expressed as follows: V_W_X_Y_Z where V is the group number; W indicates the presence and number of the vascular channels (0 indicates plain lime; 2 indicates 2 channels, 4 indicates 4 channels); X is the age of the first test in days; Y is the healing agent used to fill the channels (LS15 = lithium silicate at concentration of 15 %, LS20 = lithium silicate at concentration of 20 %, w = deionised water); Z is the level of the damage, reported in terms of crack width (CMOD equal to 0.1 mm).

### 2.5. Healing indices calculation

Healing indices were calculated using a framework previously developed by the authors [34,35,43,44] and implemented here to assess healing performance over multiple damage–healing cycles. This methodology allows two complementary evaluations: (i) recovery relative to the original undamaged state; (ii) recovery between successive cycles; (iii) evaluation of inter-cycle healing performance. The latter is crucial for understanding the long-term functionality and viability of the vascular network under repeated damage events.

As represented in Fig. 3, the results of the pre-cracked and post healed specimens are presented in terms of load vs CMOD responses. Flexural strength was determined from the peak load using the standard three-point bending equation, with a span length of 200 mm and specimen dimensions of 75 mm (width) × 75 mm (depth). Two primary indices were used to assess healing efficiency; strength recovery ($\eta_{\sigma}^{k1}$ (%)) and stiffness recovery ($\eta_{K}^{k1}$ (%)), as defined for the first healing cycle in Eqs. 2 and 3 respectively, with notation provided in Fig. 3.

$$\eta_{\sigma}^{k1} = \frac{\overline{\sigma}_{\text{healed}}^{k1} - \overline{\sigma}_{\text{damaged}}^{k}}{\overline{\sigma}_{\text{undamaged}}^{k} - \overline{\sigma}_{\text{damaged}}^{k}} \tag{2}$$

$$\eta_{K}^{k1} = \frac{\overline{K}_{\text{healed}}^{k1} - \overline{K}_{\text{damaged}}^{k1}}{\overline{K}_{\text{undamaged}}^{k} - \overline{K}_{\text{damaged}}^{k}} \tag{3}$$

For multiple healing cycles, additional indices were defined:

Cycle-to-original strength and stiffness recovery, referencing the performance at the end of the cycle with respect to the original undamaged state, for second ($\eta_{\sigma}^{k2}, \eta_{K}^{k2}$) and third cycles ($\eta_{\sigma}^{k3}, \eta_{K}^{k3}$), defined by Eqs. (4) and (5) as follows:

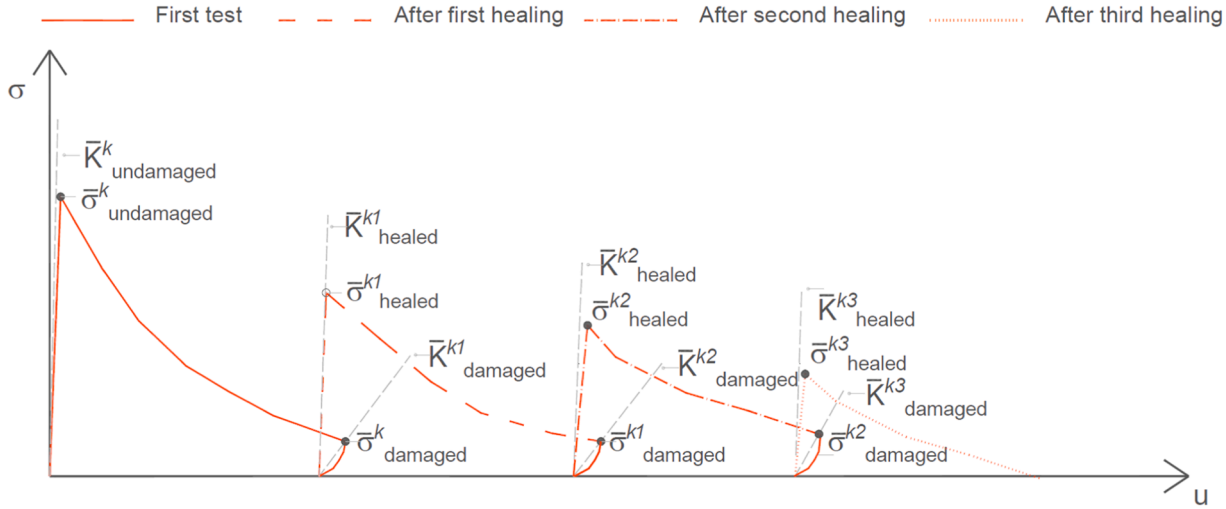


**Fig. 3.** Stress-CMOD curves before and after healing cycles: notation and definition of the parameters for the indices of healing.

**Table 1**
Experimental programme.

| | Sample designation | No. channels | | | Age of first test (days) | | | Healing agents | | | Crack width CMOD (mm) | Healing period (14 days) | | SEM |
|---|---|---|---|---|---|---|---|---|---|---|---|---|---|---|
| | | 0 | 2 | 4 | 14 | 28 | 365 | LS15 | LS20 | w | 0.1 | Single cycle | Multiple cycles | |
| GROUP 1 | 1_0_14 | ✓ | - | - | ✓ | - | - | - | - | - | - | | - | - |
| | 1_4_14_0.1 | - | - | ✓ | ✓ | - | - | - | - | - | ✓ | ✓ | - | - |
| | 1_2_14_LS15_0.1 | - | ✓ | | ✓ | - | - | ✓ | - | - | ✓ | ✓ | - | - |
| | 1_2_14_LS20_0.1 | - | ✓ | | ✓ | - | - | - | ✓ | - | ✓ | ✓ | - | - |
| | 1_4_14_LS15_0.1 | - | - | ✓ | ✓ | - | - | ✓ | - | - | ✓ | ✓ | - | - |
| | 1_4_14_LS20_0.1 | - | - | ✓ | ✓ | - | - | - | ✓ | - | ✓ | ✓ | - | - |
| GROUP 2 | 2_0_28 | ✓ | - | | - | ✓ | - | - | - | - | - | ✓ | - | - |
| | 2_4_28_0.1 | - | - | ✓ | - | ✓ | - | - | - | - | ✓ | ✓ | - | - |
| | 2_2_28_LS15_0.1 | - | ✓ | | - | ✓ | - | ✓ | - | - | ✓ | ✓ | - | - |
| | 2_2_28_LS20_0.1 | - | ✓ | - | - | ✓ | - | - | ✓ | - | ✓ | ✓ | - | - |
| | 2_4_28_LS15_0.1 | - | - | ✓ | - | ✓ | - | ✓ | - | - | ✓ | ✓ | - | - |
| | 2_4_28_LS20_0.1 | - | - | ✓ | - | ✓ | - | - | ✓ | - | ✓ | ✓ | - | - |
| GROUP 3 | 3_0_365 | ✓ | - | - | - | - | ✓ | - | - | - | - | - | - | - |
| | 3_4_365_w_0.1 | - | - | - | - | - | ✓ | - | - | ✓ | ✓ | - | ✓ | - |
| | 3_4_365_LS15_0.1 | - | - | ✓ | - | - | ✓ | ✓ | - | - | ✓ | - | ✓ | ✓ |
| | 3_4_365_LS20_0.1 | - | - | ✓ | - | - | ✓ | - | ✓ | - | ✓ | - | ✓ | ✓ |

$$\eta_{\sigma}^{k2} = \frac{\overline{\sigma}_{\text{healed}}^{k2} - \overline{\sigma}_{damaged}^{k1}}{\overline{\sigma}_{\text{undamaged}}^{k} - \overline{\sigma}_{damaged}^{k1}} \quad (4)$$

$$\eta_{K}^{k2} = \frac{\overline{K}_{\text{healed}}^{k2} - \overline{K}_{damaged}^{k1}}{\overline{K}_{\text{undamaged}}^{k} - \overline{K}_{damaged}^{k1}} \quad (5)$$

The within-cycle healing indices, highlighting the improvements achieved during each healing cycle relative to the damaged state prior to healing, are defined by the following Eqs. (6) and (7), where n is the cycle number:

$$\eta_{\sigma}^{kn-1} = \frac{\overline{\sigma}_{\text{healed}}^{kn} - \overline{\sigma}_{damaged}^{kn-1}}{\overline{\sigma}_{\text{healed}}^{kn-1} - \overline{\sigma}_{damaged}^{kn-1}} \quad (6)$$

$$\eta_{K}^{kn-1} = \frac{\overline{K}_{\text{healed}}^{kn} - \overline{K}_{damaged}^{kn-1}}{\overline{K}_{\text{healed}}^{kn-1} - \overline{K}_{damaged}^{kn-1}} \quad (7)$$

## 3. Results

### 3.1. Wettability results

Wettability results, obtained using standard glass plates to minimise surface roughness variability and ensure data comparability, are presented in Table 2. The values represent the average of three measurements, with the coefficient of variation (CoV %) shown in brackets. Since all tested healing agents are aqueous solutions, deionised water was included as a reference to account for the solvent's influence and enable a reliable comparison of wettability characteristics. Representative contact angle measurements for each healing agent are shown in Fig. 4.

Regarding contact angle measurements, LS-based solutions (LS15 and LS20) exhibit slightly higher contact angles than water, ranging from 25° to 28°. reflecting lower wettability. LS20 exhibits the highest contact angle (~28°), suggesting the lowest wettability among the three, which is consistent with its higher concentration. Contact angle values slightly decrease over the first 10 s, suggesting minor spreading of the droplet, though the changes are minimal—particularly for LS20, which maintains a relatively stable profile over time. The baseline for deionised water was slightly smaller compared to LS15 and LS20, which may indicate a stronger initial spreading tendency for the healing agents. Notably, the baseline values remained relatively stable between 0 and 10 s for all samples, suggesting minimal dynamic spreading over this short time frame. Overall, the data confirm that increasing lithium silicate concentration reduces wettability and promotes more stable droplet behaviour.

### 3.2. Three-point bend test results

Results from the flexural tests and healing indices based on Load-CMOD data are summarized in Tables 3–5. Each result represents the average of three specimens.

### 3.3. Group 1_Results

Table 3 presents the flexural test results for Group 1, along with the healing indices calculated from the experimentally obtained Load-CMOD responses. Group_1 samples were tested at 14 days, when the surface matrix had low cohesion and mechanical strength. This compromised the attachment of the knife edges needed for clip-gauge derived CMOD measurements during flexural testing. In several cases, the knife edges detached along with fragments of surface mortar, indicating poor bonding, which may have potentially contributed to the data variability observed. The presence of empty channels had no noticeable impact on mechanical performance. Samples pre-cracked to a CMOD of 0.1 mm showed no signs of autogenous healing, either in strength or stiffness indices. This result was unexpected, as early-age natural hydraulic lime typically exhibits some degree of autogenous healing over the timescales employed in this study [24,26,28]. However, the level of damage induced by extending the test to a CMOD of 0.1 mm might have exceeded the material's self-healing capacity. At this crack width, the disruption of the matrix is likely too extensive to allow for effective reprecipitation or bonding within the crack, especially in the absence of moisture-retaining or reactive agents within the channel.

Load -CMOD graphs of samples filled with LS15 and LS20 are represented in Fig. 5. In samples where the vascular networks were filled

**Table 2**
Healing agents wettability results.

| Healing agents' designation | Volume mL (CoV%) | Contact angle ($\theta_c$) deg (CoV%) | | Baseline mm (CoV%) | |
|---|---|---|---|---|---|
| | 0 s | 0 s | 10 s | 0 s | 10 s |
| Deionised water | 5 | 22.09 | 22.07 | 4.29 | 4.24 |
| LS15 | 5.10 (18) | 25.45 (8) | 25.02 (7) | 4.49 (5) | 4.48 (5) |
| LS20 | 3.58 (11) | 28.15 (6) | 27.97(5) | 4.38 (3) | 4.37 (3) |

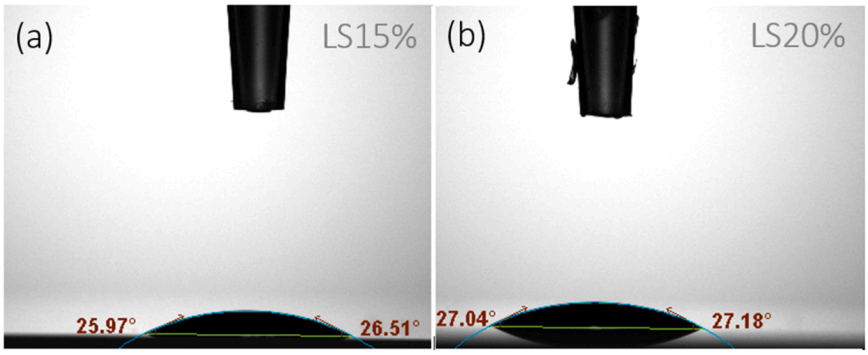


**Fig. 4.** Contact angle measurements of healing agents: Lithium silicate LS15 (a), Lithium silicate LS20 (b).

**Table 3**
Group_1: flexural test results and indices of healing.

| Group_1 | $\sigma^{k\_14}_{undamaged}$ N/mm$^2$ (CoV%) | $\sigma^{k\_14}_{damaged}$ N/mm$^2$ (CoV%) | $\sigma^{k\_28}_{healed}$ N/mm$^2$ (CoV%) | Healing indices $\eta^k_\sigma$ % | $\eta^k_K$ % |
|---|---|---|---|---|---|
| 1_0_14 | 0.72 (1) | - | | - | - |
| 1_4_14_0.1 | 0.73 (16) | 0.16 (24) | 0.13 (18) | -4 | -6 |
| 1_2_14_LS15_0.1 | 0.82(7) | 0.21(30) | 0.50(13) | 47 | 27 |
| 1_2_14_LS20_0.1 | 0.59(40) | 0.32(24) | 0.54(31) | 84 | 71 |
| 1_4_14_LS15_0.1 | 0.60(2) | 0.16(1) | 0.89(3) | 167 | 122 |
| 1_4_14_LS20_0.1 | 0.60(2) | 0.19(7) | 0.96(3) | 187 | 124 |

**Table 4**
Group_2: flexural test results and indices of healing.

| Group_2 | $\sigma^{k\_28}_{undamaged}$ N/mm$^2$ (CoV%) | $\sigma^{k\_28}_{damaged}$ N/mm$^2$ (CoV%) | $\sigma^{k\_42}_{healed}$ N/mm$^2$ (CoV%) | Healing indices $\eta^k_\sigma$ | $\eta^k_K$ |
|---|---|---|---|---|---|
| 2_0_28 | 0.97(22) | - | | - | - |
| 2_4_28_0.1 | 0.99(27) | 0.17(14) | 0.14(14) | -4 | -5 |
| 2_2_28_LS15_0.1 | 0.76(3) | 0.20(26) | 0.40(46) | 36 | 75 |
| 2_2_28_LS20_0.1 | 0.94(12) | 0.18(4) | 0.57 (8) | 51 | 101 |
| 2_4_28_ LS15_0.1 | 0.67(5) | 0.23(10) | 0.73(5) | 114 | 76 |
| 2_4_28_ LS20_0.1 | 0.70(5) | 0.18(7) | 0.45(44) | 51 | 88 |

with LS15, an interesting healing performance was observed. The healing ranged from 47 % to 167 % in strength and from 27 % to 122 % in stiffness, as the number of filled channels increased from two to four. Doubling the volume of healing agent—from two to four filled channels—resulted in more than a twofold increase in healing efficiency, both in terms of strength and stiffness. Similarly, in samples filled with LS20, increasing the number of filled channels from two to four enhanced the healing response, with strength recovery ranging from 84 % to 187 % and stiffness from 71 % to 124 %. Notably, while strength recovery was more pronounced with LS20, the maximum stiffness regains remained within a comparable range for both lithium-based solutions (LS15 and LS20), suggesting a common upper limit in stiffness recovery.

It is important to highlight that, in built heritage applications, the ideal healing agent should not significantly alter the mechanical properties of the original material. While regains exceeding 100 % may demonstrate excellent healing efficiency from a material science perspective, such performance is not necessarily desirable in the conservation of historic masonry. Excessive mechanical enhancement in the healed zones can create heterogeneities within the structure, potentially leading to local stress concentrations at the interface between healed and unhealed areas. This mismatch can compromise the long-term structural integrity of the system. Therefore, a more suitable outcome in this context is the recovery of mechanical properties to a level comparable to the surrounding original material, ensuring homogeneity and compatibility across the matrix.

### 3.4. Group 2_Results

A summary of the test results for samples cured for 28 days is provided in Table 4. Control samples—with and without empty channels—showed similar initial flexural strengths (0.97 MPa and 0.99 MPa, respectively). Compared to the results at 14 days, both sets of samples showed a 26 % increase in strength over the subsequent two weeks, regardless of the presence of empty channels. No autogenous healing was observed, as neither a regain in strength nor in stiffness was detected after a healing period of 14 days. Interestingly, samples injected with LS15 displayed notable healing performance. Strength recovery ranged from 36 % (with 2 channels) to 114 % (with 4 channels), accompanied by significant stiffness gains of 75–76 %. These results suggest that increasing the volume of LS15 markedly improves strength recovery, while stiffness gains plateau at high levels, approaching the original values. Samples treated with LS20 exhibited more consistent recovery, with stiffness ranging from 88 % (2 channels) to 101 % (4 channels) and strength consistently at 51 % for both 2 and 4 channels. The overall impact of increased volume seems to be less pronounced compared to LS15.

Despite clear trends in recovery performance, noticeable variability exists across the data, which can be attributed to the complex interactions within the NHL–lithium silicate (LS) system, as can be seen in

**Table 5**
Group_3: flexural test results strength values over three successive damage–healing cycles.

| Group_3 | First cycle $\sigma^{k\_365}_{undamaged}$ N/mm$^2$ (CoV%) | $\sigma^{k\_365}_{damaged}$ N/mm$^2$ (CoV%) | $\sigma^{k\_379}_{healed}$ N/mm$^2$ (CoV%) | Second cycle $\sigma^{k\_379}_{damaged}$ N/mm$^2$ (CoV%) | $\sigma^{k\_393}_{healed}$ N/mm$^2$ (CoV%) | Third cycle $\sigma^{k\_393}_{damaged}$ N/mm$^2$ (CoV%) | $\sigma^{k\_407}_{healedd}$ N/mm$^2$ (CoV%) |
|---|---|---|---|---|---|---|---|
| 3_0_365 | 0.93(2) | - | - | - | - | - | - |
| 3_4_365_w_0.1 | 1.04(4) | 0.33(18) | 0.17(79) | 0.11(92) | 0.10(82) | - | - |
| 3_4_365_LS15_0.1 | 1.01(13) | 0.39(6) | 0.48(8) | 0.31(12) | 0.61(6) | 0.40(6) | 0.68(5) |
| 3_4_365_LS20_0.1 | 0.93(15) | 0.33(9) | 0.41(24) | 0.24(8) | 061(27) | 0.32(6) | 0.53(27) |

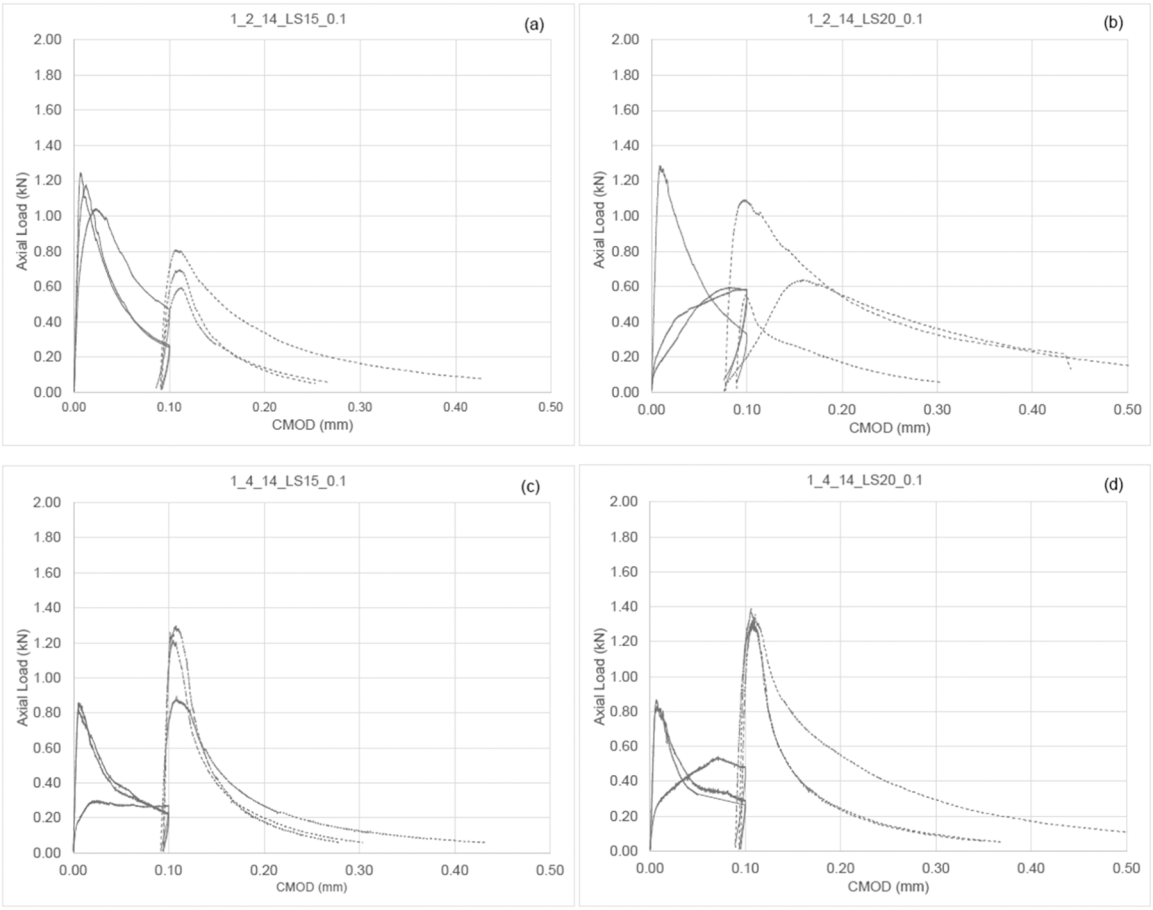


**Fig. 5.** Group_1 Load- CMOD responses of samples tested at 14 days, two vascular channels filled with LS15 (a); two vascular channels filled with LS20 (b); four vascular channels filled LS15 (c); four vascular channels filled LS20 (d).

Fig. 6. This scatter might be driven by several factors: uneven distribution of lithium silicate within the NHL matrix, differences in crack morphology, and local micro-environment variations. Central to this variability is the ongoing formation of calcium silicate hydrate (C-S-H) at 28 days. Natural hydraulic lime continues to hydrate, with $C_2S$ contributing significantly to strength over 6–12 months [90]. Meanwhile, lithium silicate reacts with residual calcium hydroxide to form C-S-H, densifying the matrix and reducing porosity, but this reaction operates on a similar timeline that overlaps with the slower NHL hydration [78].

### 3.5. Group 3_Results

Samples in Group 3 were tested after one year of curing and subjected to three consecutive damage–healing cycles. The aim was to assess the long-term healing potential of lithium silicate solutions (LS15 and LS20) when used at maximum volume (four channels), as well as their ability to support multiple damage–healing cycles over an extended curing period. Control samples tested after one year of curing confirmed the absence of autogenous healing, as expected, since this phenomenon is more pronounced at early ages [24]. Remarkably, samples filled with LS15 and LS20 demonstrated strength and stiffness recovery across all three healing cycles, as summarised in Table 6. Load–CMOD graphs of the cycles are shown in Fig. 7.

For LS15-filled samples, within-cycle strength recovery increased substantially from 13 % in the first cycle to 43 % in the second, more than tripling, and was confirmed in the third cycle with 46 %. A similar trend was observed for stiffness recovery, which reached 73 % in the first cycle, then decreased slightly to 48 % and 51 % in the second and third cycles, respectively. To better understand the material's repeatable healing potential, cycle-to-cycle recovery ratios were examined. Between the first and second cycle, strength recovery improved by 180 %, while stiffness recovery reached 72 % of the previous cycle's performance. The third cycle still showed strong performance, with 134 % strength recovery relative to the second cycle and 100 % stiffness recovery, indicating full retention of the healing capacity.

For LS20-filled samples, a similar recovery profile was observed, though with subtle differences in magnitude and consistency. Strength recovery started at 12 % in the first cycle, peaked at 54 % in the second, then slightly declined to 35 % in the third. Stiffness recovery followed a more stable trajectory: 61 %, 80 %, and 68 % across the three cycles, respectively. In LS20-treated specimens, cycle-to-cycle analysis revealed a significant increase in both strength and stiffness recovery between the first and second healing cycles (221 % and 129 %, respectively). Although strength recovery declined in the third cycle, it still remained substantial at 72 % compared to the previous cycle, while stiffness showed a smaller reduction to 86 %. It is worth noting that not all vascular channels were fully filled during the healing cycles due to blockages identified in some specimens. This likely contributed to the variability seen in the Load–CMOD responses, particularly in Fig. 7(b) where incomplete agent delivery may have limited the healing process.

For completeness, a set of samples was also tested using deionised water as the filling fluid. After one year of curing, these samples exhibited no recovery in either strength or stiffness, confirming that the aqueous phase does not activate any healing mechanism. This behaviour aligns with the chemistry of matured natural hydraulic lime mortars, in which both carbonation and hydration reactions have largely stabilised [88,90]. As a result, autogenous healing is negligible at this stage,

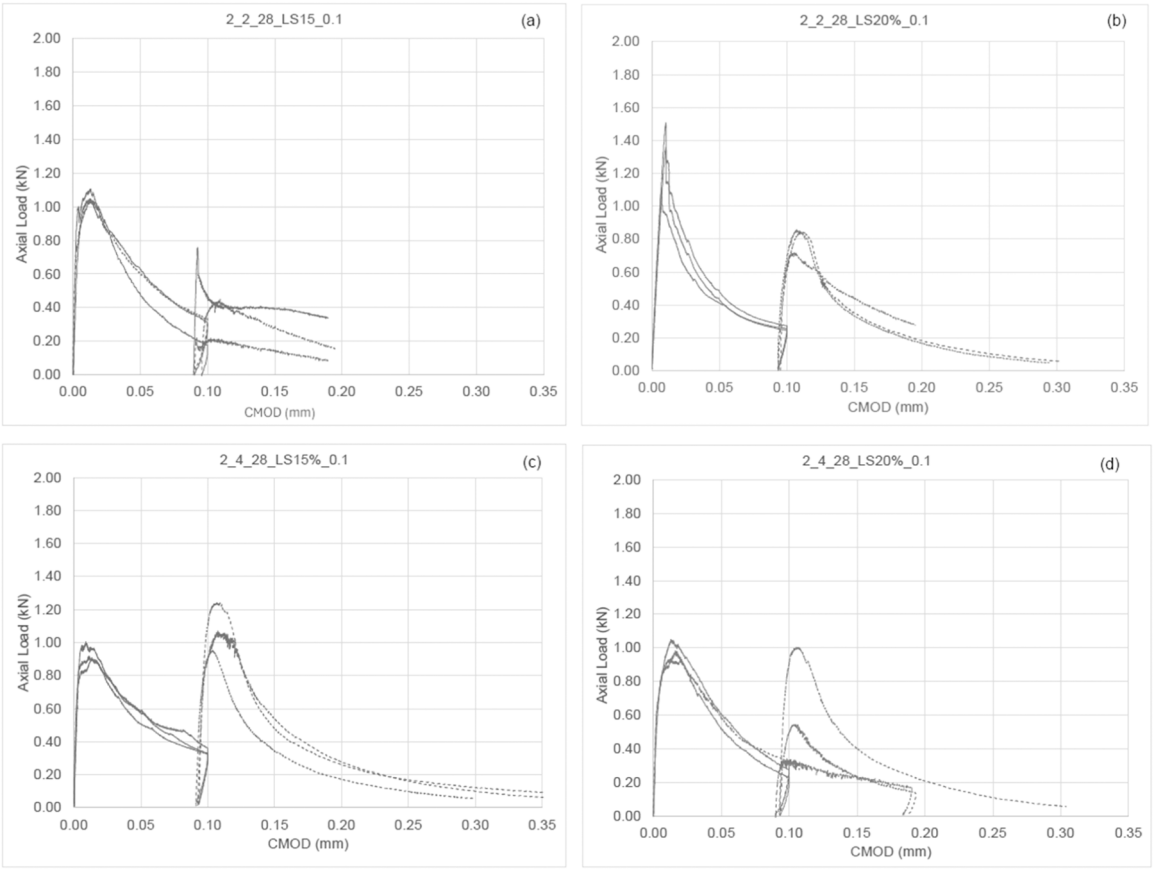


**Fig. 6.** Group_2 Load- CMOD responses of samples tested at 28 days, two vascular channels filled with LS15 (a); two vascular channels filled with LS20 (b); four vascular channels filled LS15 (c); four vascular channels filled LS20 (d).

**Table 6**
Group_3: Healing indices (%) for Group 3 samples across three consecutive healing cycles.

| Group_3 | First cycle | | Second cycle | | Third cycle | | Cycle 2–1 | | Cycle 3–2 | |
|---|---|---|---|---|---|---|---|---|---|---|
| | $\eta_{\sigma}^{k1}$ | $\eta_{K}^{k1}$ | $\eta_{\sigma}^{k2}$ | $\eta_{K}^{k2}$ | $\eta_{\sigma}^{k3}$ | $\eta_{K}^{k3}$ | $\eta_{\sigma}^{k2-1}$ | $\eta_{K}^{k2-1}$ | $\eta_{\sigma}^{k3-21}$ | $\eta_{K}^{k3-1}$ |
| 3_0_365 | - | - | - | | | | - | - | - | - |
| 3_4_365_w_0.1 | -23 | -9 | -1 | -7 | - | - | -22 | nd* | - | - |
| 3_4_365_LS15_0.1 | 13 | 73 | 43 | 48 | 46 | 51 | 180 | 72 | 134 | 102 |
| 3_4_365_LS20_0.1 | 12 | 61 | 54 | 80 | 35 | 68 | 221 | 129 | 72 | 86 |

* stiffness index was not measurable as no linear phase was found in 2/3 samples.

particularly for cracks of CMOD = 0.10 mm. These findings highlight that healing in LS-filled specimens is driven by the reactive lithium silicate component, which can promote mineral precipitation and matrix densification, processes that the aqueous phase of the solution cannot induce. The corresponding Load–CMOD response is shown in Supplementary Materials, Fig. 1.

## 4. Surface and microstructural characterisation

### 4.1. Crack surfaces observation

Fig. 8 presents cross-sectional and surface views of lime mortar specimens embedded with vascular networks, after 365 days of ageing and up to three healing cycles, for LS15, LS20, and control conditions. The sections illustrate the crack morphology, extent of lithium silicate distribution, red dots mark the locations where fragments were collected for SEM-EDS analysis. Visual inspection of fractured specimens aged 365 days, following three-point bending to failure (Section AA' and BB' in Fig. 8) revealed localised regions where the lithium silicate (LS) healing agent remained visibly unreacted 14 days after the final injection cycle. In specimens treated with LS15 unreacted agent was observed in contiguous zones across all three samples, averaging approximately 27 % of the total cross-sectional area. The vertical distribution of the agent varied slightly among samples, with observed average capillary rise of 63 mm (measured from the bottom of the samples). These values demonstrate consistent and substantial upward migration, reflecting favourable interaction between the healing agent and the NHL 3.5 pore structure. As shown in Fig. 8, sections CC′ and DD′ of Sample 1, the channels were generally empty. However, one channel in section DD′ exhibited a solidified ring with an approximate thickness of 0.005 mm,

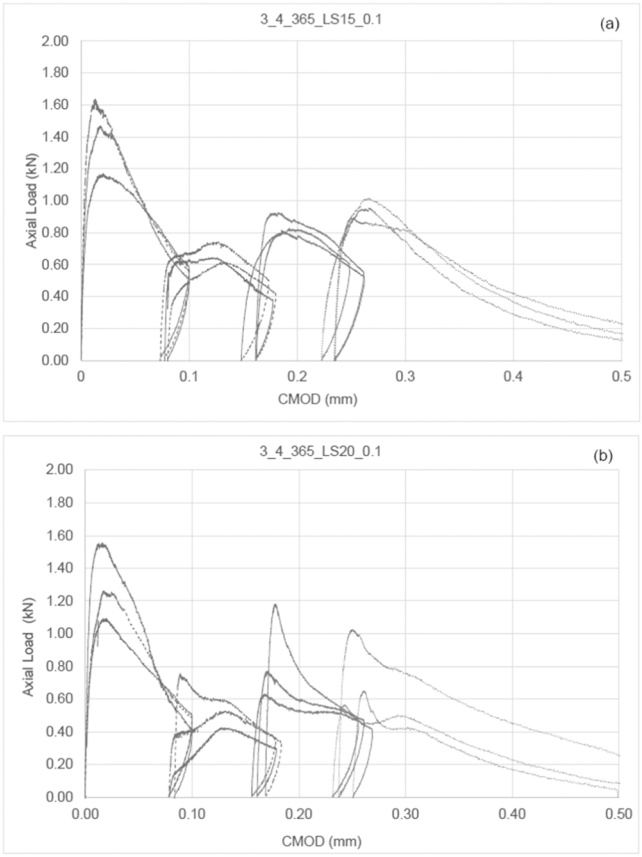


**Fig. 7.** Load–CMOD responses of Group 3 samples tested at 365 days after undergoing 3 healing cycles. Samples with four vascular channels filled with LS15 (a); samples with four vascular channels filled with LS20 (b).

reducing the cross-sectional area by only approximately 0.5 %.

In specimens treated with LS20 unreacted agent was much less prominent, observed in only one out of three samples, where it formed a finer, more fragmented unreacted areas with a vertical reach of 72 mm. This isolated instance confirms that the LS20 formulation retains good capillary mobility, despite experiencing partial blockage in other samples. As can be seen in Sample 1, sections C–C' and D–D', two out of four channels are completely clogged by the reacted agent, while one is partially blocked.

These findings confirm that capillary forces effectively mobilised and distributed the lithium silicate solutions, more efficiently in LS15 than in LS20, enabling them to access and treat internal damage zones beyond the immediate injection site. The observed vertical transport further underscores the agent's compatibility with the porous structure of NHL mortars, suggesting strong potential for autonomous delivery and homogeneous distribution—key features for long-term and repeatable self-healing performance in heritage-compatible systems.

### 4.2. SEM-EDS

Scanning electron microscopy coupled with energy-dispersive X-ray spectroscopy revealed substantial microstructural densification and compositional transformations following lithium silicate treatment (Fig. 9a-n). This behaviour is consistent with previous observations that C-S-H formation leads to microstructural densification, progressive pore refinement, and increased packing of hydration products in cementitious matrices, as reported in hydration and microstructure-evolution studies [91,92].

Untreated NHL 3.5 mortar (Figs. 9a, 9d) imaged at 500 × and 10,000 × magnification shows a granular matrix with interconnected micro-porosity and discrete crystalline phases. Quantitative EDS analysis of these regions yields a mean Si/Ca ratio of 0.177 ± 0.015, consistent with a portlandite-dominated assemblage exhibiting minimal hydraulic reaction products [93]. LS15 treatment produced marked morphological refinement (Figs. 9b, 9e), with reduced fissure networks, finer granular texture, and a denser, more uniform matrix. Corresponding EDS spectra (Fig. 9h) display an enhanced Si Kα peak, indicating increased silicate incorporation and yielding a Si/Ca ratio of 0.509 ± 0.025-a 188 % increase relative to the control. This compositional shift reflects the onset of calcium silicate hydrate (C-S-H) gel formation, consisted with early-stage silica polymerisation mechanisms [91,94]. The LS20-treated samples exhibit the most advanced transformation (Figs. 9c, 9f), characterised by densely agglomerated surfaces and minimal residual porosity at both magnifications. EDS analysis (Fig. 9i) shows further intensification of the Si Kα peak and a Si/Ca ratio of 0.787 ± 0.045, representing a 345 % increase compared to untreated mortar and approaching values typical of highly polymerised C-S-H networks [94,95].

Comparative spectra normalised to their maximum intensities (Fig. 9g) reveal systematic evolution of silicon content across treatments, while calcium signals remain comparatively stable. Peak-focused analyses (Fig. 9l for Ca Kα and 10 m for Si Kα) confirm these trends, with LS20 showing the sharpest and most intense Si peak. Quantitative Si/Ca ratios (Fig. 9n) clearly differentiate compositional domains: control within the portlandite region (Si/Ca < 0.2), LS15 within the early C-S-H formation zone, and LS20 well inside the polymerised C-S-H domain (Si/Ca 0.6–1.2) [93,95]. Together, these results demonstrate a progressive transition from portlandite-dominated matrices toward increasingly silicate-rich, C-S-H-based microstructures with higher lithium silicate concentration. This microstructural and compositional evolution aligns directly with the mechanical recovery observed in flexural testing, supporting the enhanced reactivity and pore-filling efficiency afforded by LS20.

SEM images and complete raw EDS spectra from Spectrum 1–6 are presented in Supplementary Materials, Fig. 2 to supplement and support the data shown in Fig. 9.

### 4.3. Perspectives and limitations

This study introduces an innovative application of lithium silicate—traditionally used as a consolidant—as a functional healing agent within vascular self-healing systems for heritage-compatible mortars, demonstrating its potential to promote repeatable healing in natural hydraulic lime matrices. The results confirm that both LS15 and LS20 can enhance mechanical performance through strength and stiffness recovery, particularly when applied in multiple cycles. LS15 showed superior long-term healing consistency, making it a promising candidate for cyclic self-healing applications in natural hydraulic lime mortars. These findings suggest that lithium silicates can be tailored not only for short-term mechanical recovery but also for longer-term resilience strategies in heritage conservation. Although its unit cost may be relatively high, the low required concentration (15–20 %), aqueous low viscosity (avoiding toxic solvents), straightforward application, chemical stability, and long-term reliability make lithium silicate a practical and sustainable option for heritage-compatible self-healing mortars.

However, several limitations within the experimental programme must be acknowledged. It employed a simplified configuration focused

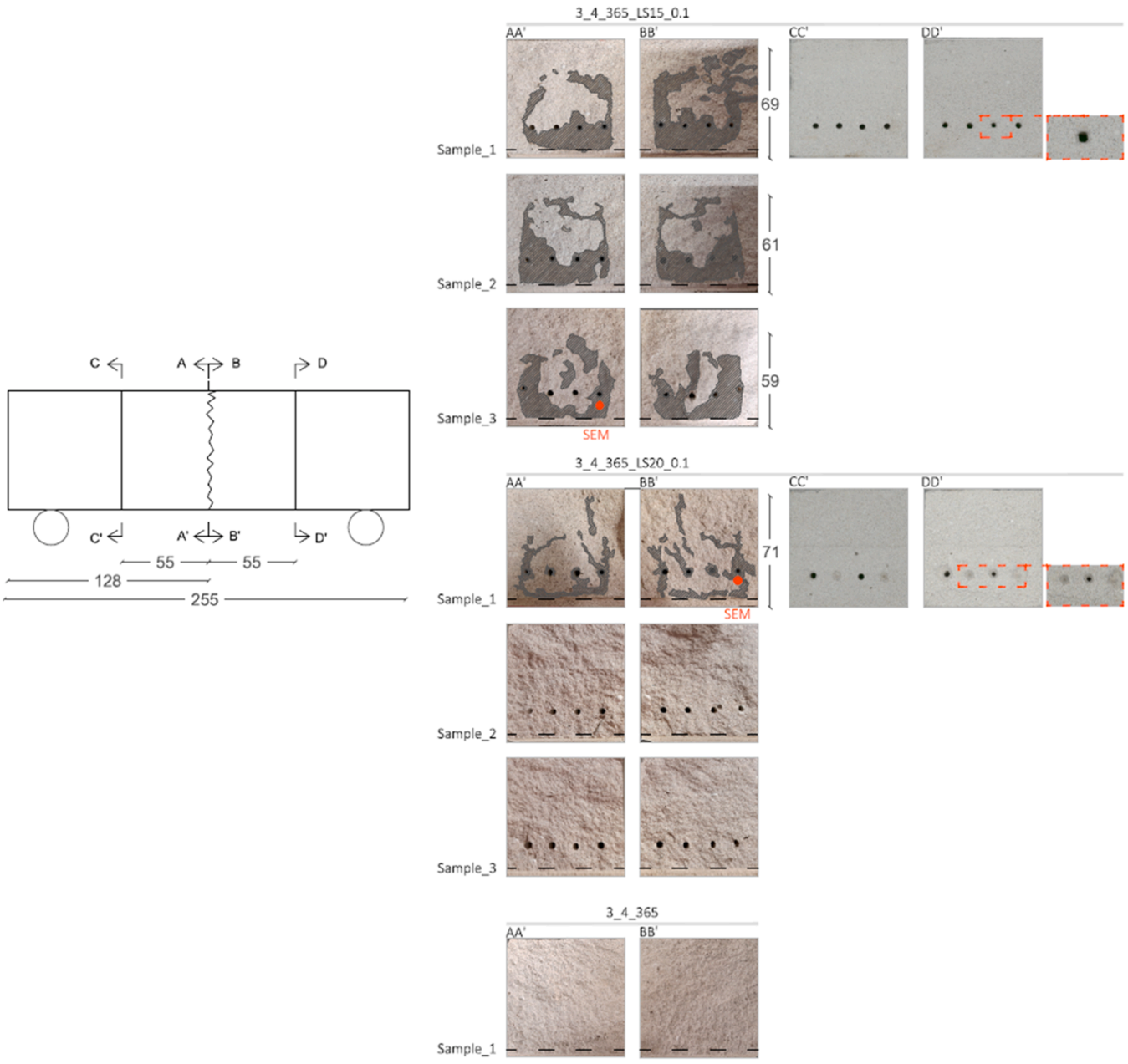


**Fig. 8.** Schematic of prismatic mortar specimens (left) and cross-sectional (AA′, BB′) and surface views (CC′, DD′) after 365 days for LS15, LS20, and control samples.

on flexural performance; the controlled 0.1 mm crack width and fixed 14-day healing period may not fully represent the range of damage scenarios in real-world applications. The study also focused on simplified vascular geometries and direct agent injection, omitting the complexities introduced by fully integrated or automated vascular systems.

While SEM–EDS observations revealed microstructural and compositional changes suggestive of calcium-silicate-hydrate (C–S–H) formation, future research will focus on confirming these findings through advanced techniques such as X-ray diffraction (XRD), Fourier-transform infrared spectroscopy (FTIR), nuclear magnetic resonance (NMR), and porosimetry analysis. These methods will enable a more comprehensive understanding of the reaction products and the evolution of pore structure within the healed matrix. While mechanical recovery indices (strength and stiffness recovery) were central to this study, future work will focus on integrating quantitative image analysis and water permeability tests to correlate morphological healing and sealing indicators with mechanical recovery, thereby offering a more comprehensive evaluation of the self-healing and self-sealing capacity of lithium silicate systems under cyclic conditions.

Additionally, the exploration of alternative vascular designs including 4D-printed, branched, or interconnected channel networks—could significantly enhance healing efficiency, delivery uniformity, and multi-crack targeting. By moving beyond simple linear channels toward refillable vascular configurations with enhanced biomimetic and spatially optimised patterns, it may be possible to better replicate the performance of natural circulatory systems and ensure a more uniform and reliable distribution of the healing agent throughout the mortar matrix. Investigating the influence of vascular geometry on

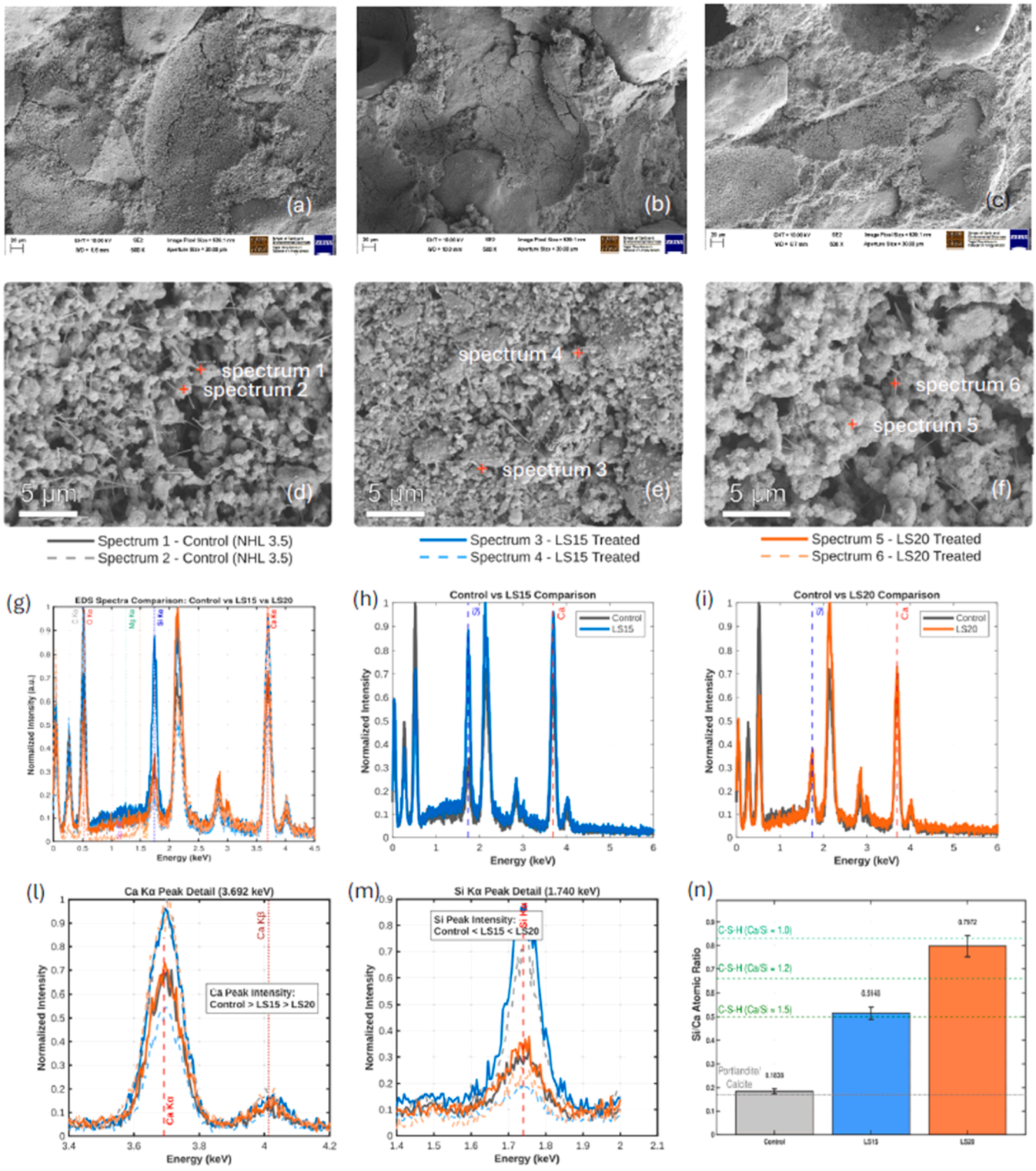


**Fig. 9.** SEM and EDS characterization of untreated and lithium-silicate-treated NHL 3.5 mortars. (a–c) Low-magnification SEM images of control, LS15, and LS20 specimens. (d–f) High-magnification SEM images showing progressive surface densification from control to LS20. (g) Comparative EDS spectra for all samples. (h–i) Detailed EDS comparisons of control vs. LS15 and control vs. LS20. (l–m) Ca Kα and Si Kα peak regions. (n) Atomic Si/Ca ratios illustrating compositional evolution with treatment.

agent flow dynamics, crack interception probability, and system robustness will be critical to improving the scalability and long-term effectiveness of vascular self-healing strategies for heritage masonry applications.

## 5. Conclusion

This study examined the cyclic self-healing performance of natural hydraulic lime (NHL) mortars incorporating vascular networks filled with lithium silicate (LS) solutions. A simplified system of empty

channels was embedded in the mortar to isolate the healing agent's intrinsic effects. Two LS concentrations were tested, LS15 and LS20, prepared from a commercial Chimica Restauri (Italy) solution. The findings highlight several key conclusions:

- the results demonstrate that plain NHL mortars exhibit negligible autogenous healing when subjected to controlled crack opening, confirming the need for engineered healing strategies in heritage-compatible materials.
- both lithium silicate solutions significantly enhanced the healing capacity of the mortars. The recovery of mechanical performance and stiffness across different curing ages indicates that lithium silicate promotes internal matrix densification and likely activates secondary hydration or related physicochemical processes that favour crack filling and bond restoration.
- a distinct concentration-dependent response was observed. While LS20 provided a strong initial healing effect in single-cycle conditions, its performance diminished over repeated cycles, suggesting that higher concentrations may prematurely seal cracks and limit further transport of the healing agent. In contrast, LS15 delivered more stable and repeatable healing across multiple cycles, indicating better long-term compatibility with cyclic healing demands.
- overall, lithium silicate—particularly the lower concentration LS15—shows strong potential as a reactive, repeatable healing agent for heritage-oriented NHL mortars. Its ability to promote microstructural densification and sustain healing over successive cycles makes it a promising candidate for long-term conservation strategies involving autonomously healing lime-based materials.

## Declaration of Competing Interest

The authors declare that they have no known competing financial interests or personal relationships that could have appeared to influence the work reported in this paper.

Cristina De Nardi reported that the research was funded by the Leverhulme Trust ECF-2022–235.

## Acknowledgements

Cristina De Nardi reported that the research was funded by the Leverhulme Trust ECF-2022–235. The authors acknowledge *CIR CHIMICA ITALIANA RESTAURI* for providing Lithium silicates.

The authors also acknowledge the considerable help and expertise of Richard Thomas, Ian King, Carl Wadsworth, F. Santoro without whom the laboratory work would not have been possible.

## Appendix A. Supporting information

Supplementary data associated with this article can be found in the online version at doi:10.1016/j.conbuildmat.2026.145154.

## Data availability

Data will be made available on request.

## References

[1] Historic England, Energy Effic. Hist. Build. Insul. Solid Walls (2016).
[2] P.F.G. Banfill, Hygrothermal simulation of building performance: data for Scottish masonry materials, Mater. Struct. /Mater. Et. Constr. 54 (2021), https://doi.org/10.1617/s11527-021-01759-x.
[3] C. Sabbioni, M. Cassar, P. Brimblecombe, R.A. Lefevre, Vulnerability Cult. Herit. Clim. Change (2009).
[4] UNESCO World Heritage Convention, Climate Change and World Heritage, (2025). ⟨https://whc.unesco.org/en/climatechange/?utm_source=chatgpt.com⟩ (accessed June 24, 2025).
[5] H. Fluck, M. Dawson, Climate change and the historic environment, Hist. Environ. Policy Pract. 12 (2021) 263–270, https://doi.org/10.1080/17567505.2021.1990492.
[6] P. Brimblecombe, Refining climate change threats to heritage, J. Inst. Conserv. 37 (2014) 85–93, https://doi.org/10.1080/19455224.2014.916226.
[7] S. O'Neill, S.F.B. Tett, K. Crowley, Extreme rainfall risk and climate change impact assessment for Edinburgh World Heritage sites, Weather Clim. Extrem 38 (2022) 100514, https://doi.org/10.1016/j.wace.2022.100514.
[8] P.R.P.J. Van Hees, L. Binda, I. Papayianni, E. Toumbakari, Rilem Techical Committe Characterisation and damage analysis of old mortars, 37 (2004).
[9] M.R. Valluzzi, F. Casarin, E. Garbin, F. Da Porto, C. Modena, Long-term damage on masonry towers case studies and intervention strategies. 11th International Conference on Fracture 2005, ICF11, 2005, pp. 3253–3256.
[10] A. Isebaert, W. De Boever, F. Descamps, J. Dils, M. Dumon, G. De Schutter, E. Van Ranst, V. Cnudde, L. Van Parys, Pore-related properties of natural hydraulic lime mortars: an experimental study, Mater. Struct. /Mater. Et. Constr. 49 (2016) 2767–2780, https://doi.org/10.1617/s11527-015-0684-5.
[11] P. Maravelaki-Kalaitzaki, A. Bakolas, I. Karatasios, V. Kilikoglou, Hydraulic lime mortars for the restoration of historic masonry in Crete, Cem. Concr. Res 35 (2005) 1577–1586, https://doi.org/10.1016/j.cemconres.2004.09.001.
[12] M.J. Mosquera, D. Benítez, S.H. Perry, Pore structure in mortars applied on restoration: Effect on properties relevant to decay of granite buildings, Cem. Concr. Res 32 (2002) 1883–1888, https://doi.org/10.1016/S0008-8846(02)00887-6.
[13] A.P. Duffy, T.P. Cooper, S.H. Perry, Repointing mortars for conservation of a historic stone building in Trinity College, Dublin, Mater. Struct. 26 (1993) 302–306, https://doi.org/10.1007/BF02472952.
[14] M.J. Mosquera, B. Silva, B. Prieto, E. Ruiz-Herrera, Addition of cement to lime-based mortars: Effect on pore structure and vapor transport, Cem. Concr. Res 36 (2006) 1635–1642, https://doi.org/10.1016/j.cemconres.2004.10.041.
[15] A. Arizzi, C. Parra-Fernández, A comprehensive review of the manufacturing process and properties of natural hydraulic limes, Mater. Struct. /Mater. Et. Constr. 58 (2025), https://doi.org/10.1617/s11527-025-02656-3.
[16] J. Lanas, J.L.P. Bernal, M.A. Bello, J.I.A. Galindo, Mechanical properties of natural hydraulic lime-based mortars, Cem. Concr. Res 34 (2004) 2191–2201, https://doi.org/10.1016/j.cemconres.2004.02.005.
[17] C.L.S. Blavier, H.E. Huerto-Cardenas, N. Aste, C. Del Pero, F. Leonforte, S. Della Torre, Adaptive measures for preserving heritage buildings in the face of climate change: A review, Build. Environ. 245 (2023) 110832, https://doi.org/10.1016/j.buildenv.2023.110832.
[18] P. Booth, L. Jankovic, Novel biodesign enhancements to at-risk traditional building materials, Front Built Environ. 8 (2022), https://doi.org/10.3389/fbuil.2022.766652.
[19] D. Lucanto, An advanced framework for regenerative design in digital and physical prototyping. crafting a comprehensive atlas for predictive modeling and adaptive technologies in climate change scenario analysis, in: A. Sayigh, A. Trombadore, G. Calcagno (Eds.), Getting to Zero - Beyond Energy Transition Towards Carbon-Neutral Mediterranean Cities: Selected Papers from the World Renewable Energy Congress Med Green Forum 2024, Springer Nature Switzerland, Cham, 2025, pp. 313–324, https://doi.org/10.1007/978-3-031-82323-7_26.
[20] S. van der Zwaag, An introduction to material design principles: damage prevention versus damage management bt - self healing materials, in: S. van der Zwaag (Ed.), An Alternative Approach to 20 Centuries of Materials Science, Springer Netherlands, Dordrecht, 2007, pp. 1–18, https://doi.org/10.1007/978-1-4020-6250-6_1.
[21] N.T. Igarashi Shin-ichi, Kunieda Minoru, Technical Committee on Autogenous Healing Cementitious Materials, 2009.
[22] C. Dry, Des. SelfGrow. SelfSens. SelfRepair. Mater. Eng. Appl. 4234 (2001) 23–29.
[23] C. Dry, Matrix cracking repair and filling using active and passive modes for smart timed release of chemicals from fibers into cement matrices, Smart Mater. Struct. 3 (1994) 118–123, https://doi.org/10.1088/0964-1726/3/2/006.
[24] C. De Nardi, A. Cecchi, L. Ferrara, A. Benedetti, D. Cristofori, Effect of age and level of damage on the autogenous healing of lime mortars, Compos B Eng. 124 (2017) 144–157, https://doi.org/10.1016/j.compositesb.2017.05.041.
[25] C. De Nardi, S. Bullo, A. Cecchi, L. Ferrara, Self-healing capacity of advanced lime mortars, Adv. Mater. Process. Technol. 2 (2016) 349–360, https://doi.org/10.1080/2374068X.2016.1191896.
[26] C. De Nardi, S. Sayadi, I. Mihai, A. Jefferson, Simulation of autogenous self-healing in lime-based mortars, Int J. Numer. Anal. Methods Geomech. (2024), https://doi.org/10.1002/nag.3870.
[27] S. Vučetić, D. Čjepa, B. Miljević, J.M. van der Bergh, O. Šovljanski, A. Tomić, E. Nikolić, S. Markov, H. Hiršenberger, J. Ranogajec, Bio-stimulated surface healing of historical and compatible conservation mortars, Materials 16 (2023), https://doi.org/10.3390/ma16020642.
[28] C. De Nardi, R. Giorgi, Mortar-mini-vascular networks filled with nanolimes: an innovative biomimetic approach for enhancing resilience in built heritage, Constr. Build. Mater. 472 (2025) 140881, https://doi.org/10.1016/j.conbuildmat.2025.140881.
[29] C. De Nardi, D. Gardner, J. Sweeney, A. Akkady, Optimisation of 4D printed mortar-mini vascular networks (m-MVNs) for built heritage preservation, Mater. Des. 254 (2025), https://doi.org/10.1016/j.matdes.2025.114118.
[30] C. De Nardi, S. Bullo, L. Ferrara, L. Ronchin, A. Vavasori, Effectiveness of crystalline admixtures and lime/cement coated granules in engineered self-healing capacity of lime mortars, Mater. Struct. /Mater. Et. Constr. 50 (2017), https://doi.org/10.1617/s11527-017-1053-3.
[31] A.I. Omoregie, C.S. Wong, A. Rajasekar, J.H. Ling, A.B. Laiche, H.F. Basri, G. Sivakumar, T. Ouahbi, Bio-based solutions for concrete infrastructure: a review

of microbial-induced carbonate precipitation in crack healing, Buildings 15 (2025), https://doi.org/10.3390/buildings15071052.
[32] S. Gowthaman, H. Koizumi, K. Nakashima, S. Kawasaki, Field experimentation of bio-cementation using low-cost cementation media for preservation of slope surface, Case Stud. Constr. Mater. 18 (2023) e02086, https://doi.org/10.1016/j.cscm.2023.e02086.
[33] A.I. Omoregie, E.A. Palombo, D.E.L. Ong, P.M. Nissom, A feasible scale-up production of Sporosarcina pasteurii using custom-built stirred tank reactor for in-situ soil biocementation, Biocatal. Agric. Biotechnol. 24 (2020) 101544, https://doi.org/10.1016/j.bcab.2020.101544.
[34] C. De Nardi, D. Gardner, D. Cristofori, L. Ronchin, A. Vavasori, T. Jefferson, Advanced 3D printed mini-vascular network for self-healing concrete, Mater. Des. 230 (2023), https://doi.org/10.1016/j.matdes.2023.111939.
[35] C. De Nardi, D. Gardner, A.D. Jefferson, Development of 3D printed networks in self-healing concrete, Materials 13 (2020) 1328, https://doi.org/10.3390/ma13061328.
[36] B. Balzano, S. Sharifi, J. Sweeney, G. Thompson, C. de Nardi, T. Jefferson, Design of an electric activation system for the smart hybrid tendons crack-closure system in concrete beams, Dev. Built Environ. 18 (2024), https://doi.org/10.1016/j.dibe.2024.100446.
[37] C. De Nardi, D. Gardner, G. Cazzador, D. Cristofori, L. Ronchin, A. Vavasori, T. Jefferson, Experimental investigation of a novel formulation of a cyanoacrylate-based adhesive for self-healing concrete technologies, Front Built Environ. 7 (2021) 1–15, https://doi.org/10.3389/fbuil.2021.660562.
[38] Y. Shields, N. De Belie, A. Jefferson, K. Van Tittelboom, A review of vascular networks for self-healing applications, Smart Mater. Struct. 30 (2021), https://doi.org/10.1088/1361-665X/abf41d.
[39] Y. Shields, T. Van Mullem, N. De Belie, K. Van Tittelboom, An investigation of suitable healing agents for vascular-based self-healing in cementitious materials, Sustain. (Switz. ) 13 (2021), https://doi.org/10.3390/su132312948.
[40] E. Tsangouri, C. Van Loo, Y. Shields, N. De Belie, K. Van Tittelboom, D.G. Aggelis, Reservoir-vascular tubes network for self-healing concrete: performance analysis by acoustic emission, digital image correlation and ultrasound Velocity, Appl. Sci. 12 (2022), https://doi.org/10.3390/app12104821.
[41] H. Huang, G. Ye, Appl. Sodium Silic. Solut. selfHeal. Agent Cem. Mater. (2011).
[42] Z. Li, L.R.De Souza, C. Litina, A.E. Markaki, A. Al-Tabbaa, A novel biomimetic design of a 3D vascular structure for self-healing in cementitious materials using Murray's law, Mater. Des. 190 (2020) 1–14, https://doi.org/10.1016/j.matdes.2020.108572.
[43] T. Selvarajoo, R.E. Davies, B.L. Freeman, A.D. Jefferson, Mechanical response of a vascular self-healing cementitious material system under varying loading conditions, Constr. Build. Mater. 254 (2020) 119245, https://doi.org/10.1016/j.conbuildmat.2020.119245.
[44] C. De Nardi, B.L. Freeman, D. Gardner, T. Jefferson, Mechanical response and predictive modelling of vascular self-healing cementitious materials using novel healing agents, Cem. Concr. Compos 142 (2023) 105143, https://doi.org/10.1016/j.cemconcomp.2023.105143.
[45] C. Joseph, A.D. Jefferson, M.B. Cantoni, Issues relating to the autonomic healing of cementitious materials, First Int. Conf. Self Heal. Mater. (2007) 1–8.
[46] C. Joseph, D. Gardner, T. Jefferson, B. Isaacs, B. Lark, Self-healing cementitious materials: a review of recent work, Proc. Inst. Civ. Eng. Constr. Mater. 164 (2011) 29–41, https://doi.org/10.1680/coma.900051.
[47] C. Joseph, A.D. Jefferson, B. Isaacs, R. Lark, D. Gardner, Experimental investigation of adhesive-based self-healing of cementitious materials, Mag. Concr. Res. 62 (2010) 831–843, https://doi.org/10.1680/macr.2010.62.11.831.
[48] A. Kanellopoulos, T.S. Qureshi, A. Al-Tabbaa, Glass encapsulated minerals for self-healing in cement based composites, Constr. Build. Mater. 98 (2015) 780–791, https://doi.org/10.1016/j.conbuildmat.2015.08.127.
[49] Z. Wan, Y. Zhang, Y. Xu, B. Šavija, Self-healing cementitious composites with a hollow vascular network created using 3D-printed sacrificial templates, Eng. Struct. 289 (2023) 116282, https://doi.org/10.1016/j.engstruct.2023.116282.
[50] C. Heath, I.P. Bond, R. Trask, K. Boba, C. Heath, I.P. Bond, R.S. Trask, D.F. Wass, Novel manufacturing method for FRP composites with a multifunctional vascular network, 2013. ⟨https://www.researchgate.net/publication/301230007⟩.
[51] Y. Zhang, P. Lu, G. Fang, B. Dong, S. Hong, Y. Wang, J. Li, S. Fan, Enhancing mechanical properties of concrete with 3D printed vascular networks via carbonation strengthening, Cem. Concr. Compos 154 (2024) 105791, https://doi.org/10.1016/j.cemconcomp.2024.105791.
[52] Y. Shields, E. Tsangouri, C. Riordan, C. De Nardi, J.R.A. Godinho, P. Antonaci, D. Palmer, A. Al-Tabbaa, T. Jefferson, N. De Belie, K. Van Tittelboom, Non-destructive evaluation of ductile-porous versus brittle 3D printed vascular networks in self-healing concrete, Cem. Concr. Compos 145 (2024), https://doi.org/10.1016/j.cemconcomp.2023.105333.
[53] T. Selvarajoo, R.E. Davies, D.R. Gardner, B.L. Freeman, A.D. Jefferson, Characterisation of a vascular self-healing cementitious material system: flow and curing properties, Constr. Build. Mater. 245 (2020) 118332, https://doi.org/10.1016/j.conbuildmat.2020.118332.
[54] R. Davies, O. Teall, M. Pilegis, A. Kanellopoulos, T. Sharma, A. Jefferson, D. Gardner, A. Al-Tabbaa, K. Paine, R. Lark, Large scale application of self-healing concrete: design, construction, and testing, Front Mater. 5 (2018) 51, https://doi.org/10.3389/fmats.2018.00051.
[55] A. Sidiq, R. Gravina, F. Giustozzi, Is concrete healing really efficient? A review, Constr. Build. Mater. 205 (2019) 257–273, https://doi.org/10.1016/j.conbuildmat.2019.02.002.
[56] V.C. Li, E. Herbert, Robust self-healing concrete for sustainable infrastructure, J. Adv. Concr. Technol. 10 (2012) 207–218, https://doi.org/10.3151/jact.10.207.
[57] E. Yen, G. Mishra, M.I. Iqbal, P. Namakiaraghi, Y. Shields, K. Van Tittelboom, N. De Belie, Y. (Amir) Farnam, Recent progress in vascularization of cementitious composites: Fundamental concepts, strategies and applications, Constr. Build. Mater. 449 (2024) 138419, https://doi.org/10.1016/j.conbuildmat.2024.138419.
[58] M.A. Ouarabi, P. Antonaci, F. Boubenider, A.S. Gliozzi, M. Scalerandi, Ultrasonic monitoring of the interaction between cement matrix and alkaline silicate solution in self-healing systems, Materials 10 (2017), https://doi.org/10.3390/ma10010046.
[59] M. Wu, B. Johannesson, M. Geiker, A review: self-healing in cementitious materials and engineered cementitious composite as a self-healing material, Constr. Build. Mater. 28 (2012) 571–583, https://doi.org/10.1016/j.conbuildmat.2011.08.086.
[60] M. Ehsan, A. Somayeh, M. H.M, A. Mohamed, Evaluation of self-healing mechanisms in concrete with double-walled sodium silicate microcapsules, J. Mater. Civ. Eng. 27 (2015) 4015035, https://doi.org/10.1061/(ASCE)MT.1943-5533.0001314.
[61] A. Pelletier, M.; Brown, R.; Shukla, A.; Bose, Self-healing concrete with a microencapsulated healing agent, (2011).
[62] P. Giannaros, A. Kanellopoulos, A. Al-Tabbaa, Sealing of cracks in cement using microencapsulated sodium silicate, Smart Mater. Struct. 25 (2016), https://doi.org/10.1088/0964-1726/25/8/084005.
[63] A. Sidiq, R.J. Gravina, S. Setunge, F. Giustozzi, Microstructural analysis of healing efficiency in highly durable concrete, Constr. Build. Mater. 215 (2019) 969–983, https://doi.org/10.1016/j.conbuildmat.2019.04.233.
[64] K. Van Tittelboom, N. De Belie, Self-healing in cementitious materials-a review, Materials 6 (2013) 2182–2217, https://doi.org/10.3390/ma6062182.
[65] J.C. Cruz, S.M. Hernandez, D.L. Trejo-Arroyo, Z. Zarhri, J. Zarate-Medina, L. F. Jimenez, M.P. Gurrola, Evaluation of self-healing in concrete with limestone coarse aggregate impregnated with Na2SiO3solution, Mater. Res Express 9 (2022), https://doi.org/10.1088/2053-1591/ac513d.
[66] I. Capasso, A. Colella, F. Iucolano, Silica-based consolidants: Enhancement of chemical-physical properties of Vicenza stone in heritage buildings, J. Build. Eng. 68 (2023) 106124, https://doi.org/10.1016/j.jobe.2023.106124.
[67] A. Colella, I. Capasso, F. Iucolano, Comparison of latest and innovative silica-based consolidants for volcanic stones, Materials 14 (2021), https://doi.org/10.3390/ma14102513.
[68] Y. Duan, H. Pfeiffer, B. Li, I.C. Romero-Ibarra, D.C. Sorescu, D.R. Luebke, J. W. Halley, CO2 capture properties of lithium silicates with different ratios of Li2O/SiO2: an ab initio thermodynamic and experimental approach, Phys. Chem. Chem. Phys. 15 (2013) 13538–13558, https://doi.org/10.1039/c3cp51659h.
[69] A. Thorn, Lithium silicate consolidation of wet stone and plaster. 12th International Congress on the Deterioration and Conservation of Stone Columbia University, New York, USA, 2012.
[70] B. Middendorf, J.J. Hughes, K. Callebaut, G. Baronio, I. Papayianni, Investigative methods for the characterisation of historic mortars - Part 1: mineralogical characterisation, Mater. Struct. /Mater. Et. Constr. 38 (2005) 761–769, https://doi.org/10.1617/14281.
[71] C.N.A. Sleiman, X. Shi, D.G. Zollinger, An approach to characterize the wearability of concrete pavement surface treatments, Transp. Res Rec. 2673 (2019) 230–239, https://doi.org/10.1177/0361198118821668.
[72] Z. Song, Z. Lu, Z. Lai, The effect of lithium silicate impregnation on the compressive strength and pore structure of foam concrete, Constr. Build. Mater. 277 (2021) 122316, https://doi.org/10.1016/j.conbuildmat.2021.122316.
[73] S.T. Witzleben, Acceleration of Portland cement with lithium, sodium and potassium silicates and hydroxides, Mater. Chem. Phys. 243 (2020) 122608, https://doi.org/10.1016/j.matchemphys.2019.122608.
[74] K. Van Tittelboom, Self-healing concrete through incorporation of encapsulated bacteria- or polymer-based healing agents ('Zelfhelend beton door incorporatie van ingekapselde bacteri, Ugent (2012). ⟨https://biblio.ugent.be/publication/4337092⟩.
[75] J. Zhang, Y. Dai, J. Xu, J. Feng, K. Ma, The influence of the different cementitious material on self-healing of microcracks in shotcrete, Adv. Mater. Sci. Eng. 2022 (2022) 3031048, https://doi.org/10.1155/2022/3031048.
[76] B.F. Yip, E.H. Kasiman, A.R. Zainal Abidin, C.S. Tan, A. Sulaiman, Improving capillary flow predictions in self-healing concrete: a dynamic contact angle approach using the volume of fluid model, J. Build. Pathol. Rehabil. 10 (2025), https://doi.org/10.1007/s41024-025-00663-z.
[77] A. Jefferson, T. Selvarajoo, B. Freeman, R. Davies, An experimental and numerical study on vascular self-healing cementitious materials. MATEC Web of Conferences, EDP Sciences, 2019, https://doi.org/10.1051/matecconf/201928901004.
[78] Z. Song, Z. Lu, Z. Lai, Mechanical and durability performance improvement of natural hydraulic lime-based mortars by lithium silicate solution, Materials 13 (2020) 1–14, https://doi.org/10.3390/ma13225292.
[79] Y.W. Choi, C.G. Kim, E.J. Nam, S.R. Oh, An experimental study on the healing performance of complex capsules using multiphase inorganic materials for crack self-healing of cement mortars, Materials 15 (2022), https://doi.org/10.3390/ma15248819.
[80] A. Stepien, P. Kostrzewa, R. Dachowski, Influence of barium and lithium compounds on silica autoclaved materials properties and on the microstructure, J. Clean. Prod. 236 (2019) 117507, https://doi.org/10.1016/j.jclepro.2019.06.338.
[81] Z. Song, Z. Lu, Z. Lai, The effect of lithium silicate impregnation on the compressive strength and pore structure of foam concrete, Constr. Build. Mater. 277 (2021), https://doi.org/10.1016/j.conbuildmat.2021.122316.
[82] L. Kalina, V. Bílek, M. Sedlačík, V. Cába, J. Smilek, J. Fládr, Physico-chemical properties of lithium silicates related to their utilization for concrete densifiers, Materials 16 (2023), https://doi.org/10.3390/ma16062173.

[83] A. Stepien, P. Kostrzewa, R. Dachowski, Influence of barium and lithium compounds on silica autoclaved materials properties and on the microstructure, J. Clean. Prod. 236 (2019) 117507, https://doi.org/10.1016/j.jclepro.2019.06.338.
[84] I. Prasetia, S. Asano, K. Torii, Diffusion Properties of Sodium and Lithium Silicates through Cement Pastes and its Mitigating Effect on Alkali-silica Reaction, n.d.
[85] D. Robert, J. Tony, G. Diane, Development and testing of vascular networks for self-healing cementitious materials, J. Mater. Civ. Eng. 33 (2021) 04021164, https://doi.org/10.1061/(ASCE)MT.1943-5533.0003802.
[86] A. Moropoulou, A.S. Cakmak, G. Biscontin, A. Bakolas, E. Zendri, Advanced Byzantine cement based composites resisting earthquake stresses: the crushed brick/lime mortars of Justinian's Hagia Sophia, Constr. Build. Mater. 16 (2002) 543–552, https://doi.org/10.1016/S0950-0618(02)00005-3.
[87] D. Marastoni, A. Benedetti, L. Pelà, G. Pignagnoli, Torque Penetrometric Test for the in-situ characterisation of historical mortars: fracture mechanics interpretation and experimental validation, Constr. Build. Mater. 157 (2017) 509–520, https://doi.org/10.1016/j.conbuildmat.2017.09.120.
[88] L. Garijo, X. Zhang, G. Ruiz, J.J. Ortega, Age effect on the mechanical properties of natural hydraulic and aerial lime mortars, Constr. Build. Mater. 236 (2020), https://doi.org/10.1016/j.conbuildmat.2019.117573.
[89] British Standard, BS EN 12390-5:2019 BS EN 12390-5:2019 Testing hardened concrete, Brusseles, 2019.
[90] C. Groot, R. Veiga, I. Papayianni, R. Van Hees, M. Secco, J.I. Alvarez, P. Faria, RILEM TC 277-LHS report: lime-based mortars for restoration–a review on long-term durability aspects and experience from practice, M. Stefanidou (2022), https://doi.org/10.1617/s11527-022-02052-1.
[91] H.M. Jennings, A model for the microstructure of calcium silicate hydrate in cement paste, Cem. Concr. Res 30 (2000) 101–116, https://doi.org/10.1016/S0008-8846(99)00209-4.
[92] X. Zhu, I.G. Richardson, P. Purnell, Morphology-structural change of calcium silicate hydrates, The University of Leeds, 2021.
[93] H.F.W. Taylor, Cement chemistry, 2nd edition, London, 1997.
[94] I.G. Richardson, The calcium silicate hydrates, Cem. Concr. Res 38 (2008) 137–158, https://doi.org/10.1016/j.cemconres.2007.11.005.
[95] S. Tang, Y. Wang, Z. Geng, X. Xu, W. Yu, H. A, J. Chen, Structure, fractality, mechanics and durability of calcium silicate hydrates, Fractal Fract. 5 (2021), https://doi.org/10.3390/fractalfract5020047.